THE JOURNAL OF PHYSICAL CHEMISTRY C

pubs.acs.org/JPCC Article

Effects of the Filler Property, Electron−Phonon Coupling on Thermal Conductivity, and Strain Rate on the Mechanical Property of Polyethylene Nanocomposites

Bo Zhang, Yunmin Liang, Wei Liu, and Zhichun Liu*

Cite This: J. Phys. Chem. C 2020, 124, 26001−26011 Read Online

ACCESS | Metrics & More | Article Recommendations | Supporting Information

ABSTRACT: Electron−phonon interaction (EPI) plays an important role in the transport property of metals. Nevertheless, EPI in polymer nanocomposites containing metal fillers has not been fully investigated due to the complicated physical mechanisms. In this work, the copper−polyethylene (Cu−PE) nanocomposite is used as a model system, and nonequilibrium molecular dynamics (NEMD) simulation combined with the two-temperature model (TTM) is conducted to reveal the role of EPI in Cu−PE systems. The effects of filler length, filler property, and EPI strength on thermal conductivity are revealed. A dimensionless number (Θ) is defined to characterize the electron−phonon nonequilibrium (EPN) degree. The results show that the EPN degree has a significant impact on thermal conductivity. When the system is in a strong EPN state, the effects of EPI on thermal conductivity can be negligible. However, when the EPN degree gradually decreases, ignoring EPI can severely underestimate the thermal conductivity. Furthermore, the temperature profile of electrons and phonons is extracted and the equivalent thermal circuit is presented. The additional thermal resistances induced by the nonlocal and nonequilibrium effects are revealed. Phonon spectra analysis and heat current decomposition are performed to uncover the underlying mechanisms. In addition, the effects of atomic mass density and filler types on thermal conductivity are revealed. Stress−strain simulation is conducted to unravel the effects of strain rates on the mechanical property. The results are useful for designing polymer nanocomposites with controlled thermal conductivity.

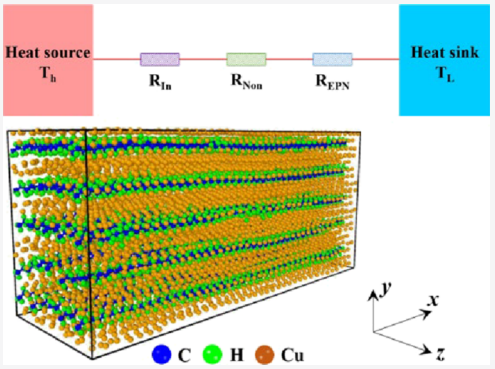

1. INTRODUCTION

Polymers have been widely used in industry owing to low cost, low density, corrosion resistance, and easy of processing.[1,2] However, thermal conductivities of bulk polymers are often below 0.5 W m^{-1} K^{-1}, which impedes heat dissipation in microelectronics.[3] Thermal conductive polymers can be used to manufacture plastic heat exchangers, which can operate in corrosive environments. In addition, thermal conductive polymers hold significant potential as thermal interface materials, which is essential to thermal management of electronic and optoelectronic devices.[4,5] Due to the mechanical robustness, polymers are promising candidates for flexible electronics and thermoelectrics.

Incorporating thermal conductive fillers into the polymer matrix is a common way to enhance the thermal conductivity of polymers. Metals such as Cu, silver (Ag), gold (Au), and nickel (Ni) are good candidates owing to superior thermal transport characteristics.[6] Through first-principles calculations, Tong et al.[7] and Giri et al.[8] found that phonons contribute little to the thermal conductivity of metals and electron−phonon coupling is sensitive to the electronic structure of a metal. Electron−phonon coupling has gained intensive attention in the process of laser manufacturing owing to the strong electron−phonon nonequilibrium (EPN).[9,10] With the development of thermometry, electron−phonon interaction (EPI) gradually received attention in noncontact photothermal measurements including Raman spectroscopy[11] and pump−probe spectroscopy.[12,13] The same focus of these studies is the time scales of EPI, which are on the order of 1 ps.[14] Nevertheless, the length scales of EPI should also be focused especially when the size of the system is comparable to the mean free path (MFP) or the EPN length of energy carriers. Mode-by-mode analysis for EPI based on first-principles is accurate but computationally expensive, which is unfeasible to polymer nanocomposites.[15,16] The two-temperature model (TTM) considers electrons and phonons as two individual systems, whose interaction is described by the electron−phonon coupling parameter. Ruan et al. found that the TTM is not suitable for graphene due to the high Debye temperature

Received: August 16, 2020
Revised: November 1, 2020
Published: November 13, 2020

https://dx.doi.org/10.1021/acs.jpcc.0c07489
J. Phys. Chem. C 2020, 124, 26001−26011

and nonequilibrium among different phonon branches.[17] However, the Debye temperature of metals is low,[18] and thus, the TTM can be applied in metal-based polymer nanocomposites.

Over the past decades, plenty of researchers have devoted their attention to the thermal transport of polymers. Henry and Chen found that the thermal conductivity of a single polyethylene (PE) chain can be divergent via molecular dynamics (MD) simulation,[19] which is associated with cross-correlations of mid-frequency phonons.[20] They also found that the thermal conductivity of PE decreases with the increase of system dimension.[21] Liu and Yang found that thermal conductivities of polymers intimately depend on the monomer type[22] and can be tuned using mechanical strain.[23] Using the first-principles-based lattice dynamics, Wang et al. observed that the thermal conductivity of a single PE chain and bulk PE crystals can be 1400 and 237 W m^{-1} K^{-1}, respectively.[24] By considering nuclear quantum motion, Shulumbda et al.[25] found that the thermal conductivity of PE crystals is around 160 W m^{-1} K^{-1}. Liao et al. found that heavy atoms can hinder phonon transport along PE chains[26] while aligning PE chains is beneficial to phonon transport.[27] Tu et al. found that torsion and tension can be combined to enhance the thermal conductivity of PE chains.[28] Ma et al.[29,30] and Luo et al.[31] found that branched chains can induce more phonon scattering. Luo et al. found that thermal conductivities of polymers are strongly related to the backbone strength[32] and the spatial extension of polymer chains.[33,34] Yang et al. investigated the impacts of doping,[35] strain,[36] water content,[37] and degree of crystallinity[38] on the thermal conductivity of polymers. In experiments, Chen et al. fabricated thermal-conductive PE nanofibers[39,40] and PE thin films[41] via stretching and shearing methods. Through electrospinning, Li et al. investigated the impacts of the molecular weight, side groups,[42] and external electric field[43] on the thermal conductivity of electrospun nanofibers. Through tuning hydrogen interaction, Mu et al.[44] and Zhang et al.[45] effectively enhanced the thermal conductivity of poly(vinyl alcohol) and nylon. Using transient grating spectroscopy, Robbins et al. observed that the phonon MFP of semicrystalline PE films can be up to 200 nm.[46] Cahill et al.[47] and Cao et al.[48] found that higher orientation of polymer chains can lead to better thermal transport. Kodama et al.[49] found that encapsulating fullerene in carbon nanotubes can effectively tune the thermal conductivity.

Previous studies have fully investigated the structural property relationships of pure polymers and polymer nanocomposites, but bulk polymer nanocomposites with expected thermal conductivity are still in demand. With the advance of computational methods, MD simulation is a powerful tool in investigating micro/nanoscale heat transfer.[50] Nanoscale spatial confinement can align polymer chain orientation, and the nanopore structure can effectively affect phononic thermal conductivity with few impacts on electrical conductivity. Thus, encapsulating the polymer chain in a secondary material is a promising way to fabricate novel functional materials for electronics and thermoelectrics. In the current paper, the effects of the filler length, filler property, and electron−phonon coupling on the thermal conductivity of polymer nanocomposites are unveiled. We find that the EPN degree plays a crucial role in the thermal conductivity, and a pivotal EPN dimensionless number is defined. The nonlocal and the nonequilibrium effects of energy carriers can generate additional thermal resistance. Phonon spectra analysis and heat current spectral decomposition manifest that the EPN degree can directly influence the low-frequency phonons. Moreover, we find that the impact of strain rates on the mechanical modulus is small and doping heavier atoms reduces thermal conductivity more.

2. MODEL AND METHODS

The stereoscopic view of Cu−PE is shown in Figure 1a. The main view and the lateral view of Cu−PE are shown in Figure S1 (Supporting Information). First, a Cu lattice is created and replicated two times along the y and z directions, respectively. Second, Cu atoms inside the lattice are removed to form a hole, whose size is around 3.615 × 3.615 × 3.615 Å^3. Third, an ethylene unit is inserted into the hole to form a Cu−PE unit. Then, the Cu−PE unit is replicated five times along the y and z directions to form a bigger Cu−PE unit. With the help of nanoscale confinement, the current Cu−PE system combines the strength of PE chains and metal fillers. Cu−PE systems of different lengths are produced by replicating Cu−PE units along the x direction. Figure S2 shows the schematic diagram of building a Cu−PE system. For building Cu-PE systems with 13,000 and 97,500 atoms, the Cu-PE unit is replicated 40 and 300 times along the x direction, respectively. For Ni−PE, Ag−PE, and Au−PE, the building process is the same as that of Cu−PE except for the different metal fillers. The initial Cu−PE system first experiences energy minimization and then equilibrates in the isothermal−isobaric (NPT) ensemble for 10 ns to fully reach thermodynamic equilibrium. During equilibration, the energy, volume, and density evolution are monitored, and the results are shown in Figure S3 (Supporting Information). The temperature and pressure are controlled at 300 K and 1 atm via a Nosé−Hoover thermostat and a barostat, respectively. The time step is set as 0.25 fs to guarantee simulation accuracy, and the cutoff distance is set as 10 Å. All of the simulations are conducted using the Large-scale Atomic/Molecular Massively Parallel Simulator

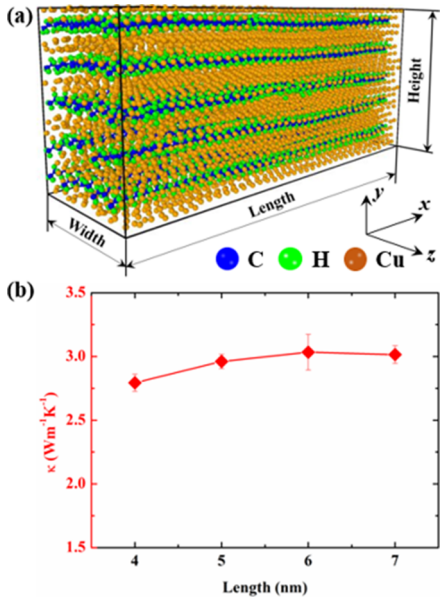

Figure 1. (a) Three dimensional view of Cu−PE. (b) Thermal conductivity of Cu−PE versus the length of the establishing temperature gradient (L_T).

https://dx.doi.org/10.1021/acs.jpcc.0c07489
J. Phys. Chem. C 2020, 124, 26001−26011

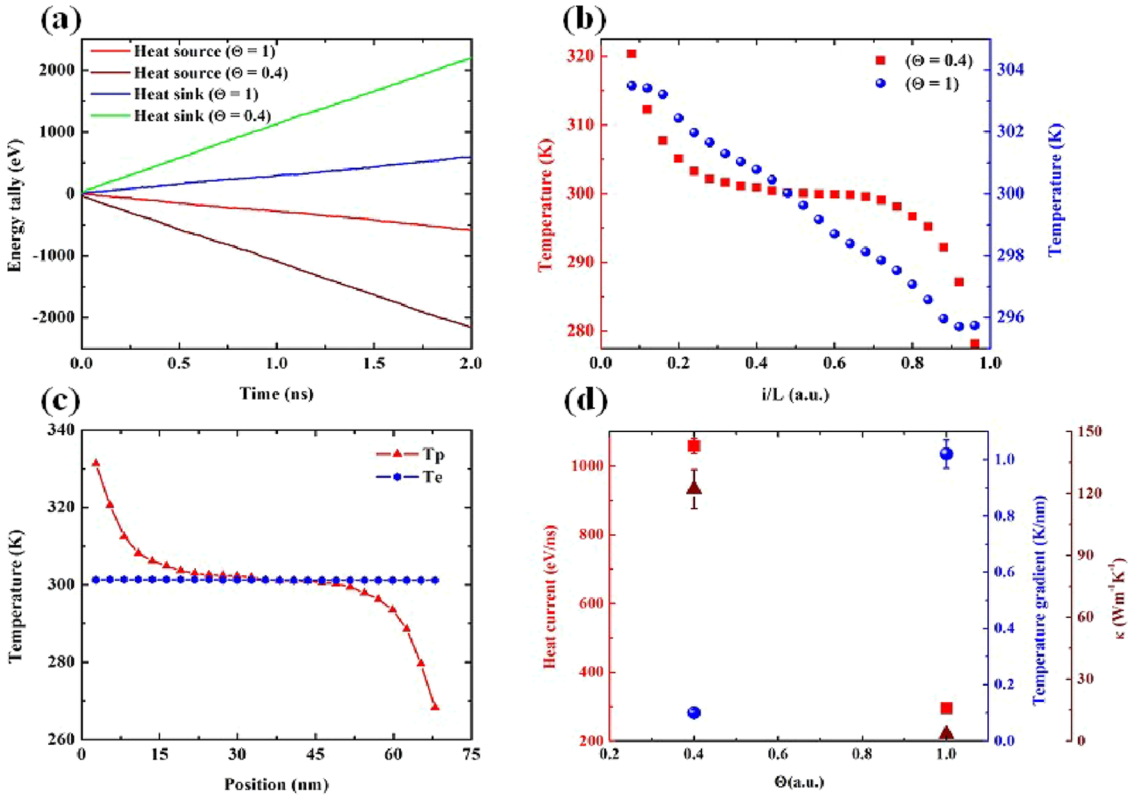

Figure 2. (a) Energy tallies of heat reservoirs as a function of time and electron−phonon nonequilibrium degree. (b) Steady-state temperature distribution as a function of time and electron−phonon nonequilibrium degree. (c) Temperature of electrons and phonons in weak electron−phonon nonequilibrium degree (Θ = 0.4). (d) Heat current, temperature gradient, and thermal conductivity of Cu−PE as functions of electron−phonon nonequilibrium degree.

(LAMMPS) package.[51] The Velocity Verlet algorithm is used to integrate the equation of atomic motion, and periodic boundary conditions are applied in all three directions. After NPT equilibration, the system continues to equilibrate in the canonical (NVT) ensemble for 1 ns and the temperature is controlled at 300 K using a Nosé−Hoover thermostat. The structural parameters of equilibrium PE nanocomposites are listed in Table S1 (Supporting Information). Later, the thin layers (5 Å) at each end of the system are fixed to hinder the heat transfer across the boundary and translational drift of the system. The 10 Å-thick layers next to the fixed layers are used as the heat source (304 K) and heat sink (296 K) with temperature controlled using Langevin thermostats. Then, the system runs in the NVE ensemble for 8 ns to reach the nonequilibrium steady state. The steady-state heat current Q is calculated as

$$Q = \frac{1}{2}\left(\left|\frac{dE_{in}}{dt}\right| + \left|\frac{dE_{out}}{dt}\right|\right) \quad (1)$$

where E is the energy tally of the heat source and heat sink. The temperature (T) is calculated based on the energy equipartition theorem, and the temperature gradient (∇T) is calculated by linear fitting the temperature distribution away from thermostats. Hence, the thermal conductivity (κ) is calculated according to Fourier's law

$$\kappa = -Q/(S\nabla T) \quad (2)$$

where S is the cross-sectional area. The final thermal conductivity is averaged over at least 4 simulations with different initial conditions.

The embedded-atom method (EAM) is widely used for metals including Cu, Ag, Au, and Ni. Therefore, the EAM potential is adopted to describe the interaction among metal atoms, which can be written as follows:[52]

$$U_i = \frac{1}{2}\sum_{j\neq i}\phi(r_{ij}) + F(\rho_{h,i}) \quad (3)$$

where U_i, $\phi(r_{ij})$, and $F(\rho_{h,i})$ are the potential energy, pairwise potential between atoms i and j separated by the distance r_{ij}, and the embedding potential. For PE, the accurate PCFF (Polymer Consistent Force Field) potential[53] consisting of bond, angle, dihedral, improper, and nonbonding terms is used to describe the interatomic interaction. The interaction between Cu and PE is modeled by the Lennard-Jones potential, and the parameters are chosen from the universal force field.[54] The detailed parameters of the potential energy function are shown in Section 2 of the Supporting Information.

The TTM is used to consider EPI in metals, which models the coupled electronic and phononic thermal transport by the following two heat diffusion equations:[55]

$$C_e\frac{\partial T_e}{\partial t} = \nabla\cdot(\kappa_e\nabla T_e) - G_{ep}(T_e - T_p) \quad (4)$$

$$C_p\frac{\partial T_p}{\partial t} = \nabla\cdot(\kappa_p\nabla T_p) + G_{ep}(T_e - T_p) \quad (5)$$

where C_e, T_e, κ_e, and C_p, T_p, κ_p are volumetric specific heat, temperature, and thermal conductivity for electrons and phonons, respectively. G_{ep} is the EPI parameter, and we adopted the value from Ruan's work,[56] that is, $C_e = 5.26 \times 10^4$

https://dx.doi.org/10.1021/acs.jpcc.0c07489
J. Phys. Chem. C 2020, 124, 26001−26011

J m^{-3} K^{-1}, G_{ep} = 5.5 × 10^{16} W m^{-3} K^{-1}, and κ_e = 401 W m^{-1} K^{-1}. Phononic thermal transport (eq 5) is modeled by the usual MD. Thus, phononic parameters including C_p and κ_p are computed implicitly by MD. In TTM-MD simulation, the Langevin thermostat is used to couple the electronic and phononic subsystems, which can be given by

$$m_i\dot{\boldsymbol{v}}_i = \boldsymbol{F}_i(t) - \gamma_i\boldsymbol{v}_i + \boldsymbol{F}_r(t) \tag{6}$$

where m_i, $\boldsymbol{v}_i$, and $\boldsymbol{F}_r(t)$ indicate the atomic mass, velocity, and random fluctuating force. γ_i is the friction constant associated with the EPI, which can be written as

$$\gamma_i = m_i G_{ep}/(3n_i k_B) \tag{7}$$

where n_i and k_B are the atomic number density and Boltzmann constant, respectively.

In NEMD simulation, when the length of the establishing temperature gradient (L_T) is comparable to the MFP of energy carriers, the size effects will occur. Hence, we check the size effects by changing L_T, and the results are shown in Figure 1b. The Cu−PE system overcomes the size effects successfully when L_T is around 7 nm and the thermal conductivity of Cu−PE is 3.01 ± 0.07 W m^{-1} K^{-1}. The classical MD simulation ignores electronic thermal conductivity, and the nanopore structure reduces phononic thermal conductivity. In addition, the interaction between the PE chain and Cu induces more phonon scattering. These factors make the thermal conductivity of PE−Cu lower than that of pure Cu or PE chains.

3. RESULTS AND DISCUSSION

3.1. Effects of Filler Length. The effects of filler length on the thermal conductivity are first studied by extending the length of a Cu−PE system. For TTM-MD in LAMMPS,[51] the atomic subsystem is modeled by classical MD, while the electronic subsystem is modeled as a continuum on a regular grid. Energy can be transferred spatially within the grid representing the electrons, which can also be transferred between the electronic and the atomic subsystems. The electronic temperature is represented by the temperature of the grid point and thus can be extracted. Using θ to denote the local temperature difference of electrons and phonons, Ruan et al.[55] defined the EPN characteristic length L_{NE} as the distance between the position of θ_{max} and 5% θ_{max}:

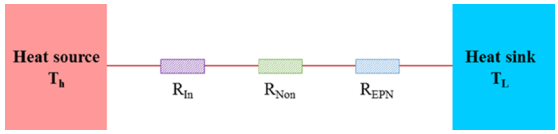

Figure 3. Equivalent thermal circuit of the Cu−PE system.

$$L_{NE} \approx \frac{3\sqrt{\kappa_e\kappa_p}}{\sqrt{G_{ep}(\kappa_e + \kappa_p)}} \tag{8}$$

For metals, the typical EPN length is on the order of 100 nm. However, the importance of the EPN length depends on the system length. To characterize the EPN degree, we further define a dimensionless number (Θ),

$$\Theta = L_{NE}/L_T \tag{9}$$

which can be used to evaluate the nonequilibrium effects between electrons and phonons. Another crucial dimensionless number in nanoscale heat transfer is the Knudsen number (K_n):

$$K_n = \Lambda/L_T \tag{10}$$

where Λ is the MFP of energy carriers. The Knudsen number can be used to evaluate the importance of nonlocal effects. In the following, we demonstrate that both the nonequilibrium and nonlocal effects of energy carriers impede thermal transport, whose roles can be regarded as the additional thermal resistances.

Figure 2a,b shows the energy tallies and steady temperature distribution of two Cu−PE systems, whose length is 9.8 and 69.83 nm, respectively. The corresponding EPN number (Θ) of two systems is 1.0 and 0.4. The energy tallies of heat reservoirs steadily increase with the increase of time, which signifies that the Cu−PE systems reach the nonequilibrium steady state. Figure 2c shows the temperature distribution of electrons and phonons when Θ is 0.4. Figure 2d shows the heat current, temperature gradient, and thermal conductivity of Cu−PE for different EPN numbers. When Θ is 1.0, the thermal conductivity of Cu−PE is 3.36 ± 0.08 W m^{-1} K^{-1}. When Θ is reduced to 0.4, the thermal conductivity can be increased to 122.13 ± 9.49 W m^{-1} K^{-1}. The effective enhancement of thermal conductivity can be understood with the help of the equivalent thermal circuit in Figure 3. The total thermal resistance consists of three parts:

$$R = R_{In} + R_{Non} + R_{EPN} \tag{11}$$

R_{In} stems from the phonon−phonon scattering and phonon-defect scattering of Cu−PE. R_{Non} stems from the nonlocal effects of electrons due to the ballistic transport of electrons. R_{EPN} stems from the EPN effects due to the small dimension. Sverdrup et al.[57] found that the nonequilibrium effects could increase the total thermal resistance of the membrane by 56%. Hence, enough attention should be paid to the EPN effects when the length of metal fillers is comparable to the nonequilibrium length. When Θ reduces from 1.0 to 0.4 owing to the extension of the system length, R_{Non} and R_{EPN} are efficiently decreased.

3.2. Effects of Electron−Phonon Coupling. For Cu, the electron−phonon coupling factor is on the order of 10^{16} W m^{-3} K^{-1}, and the electron−phonon coupling factor of metals can be tuned by changing the electronic structure.[9] In addition, our goal is to investigate the impacts of the EPN degree on thermal conductivity. Therefore, we choose to fix the dimension of the system and tune the EPI strength. Figure 4a,b displays the energy tallies of heat reservoirs and steady-state temperature distribution vary with electron−phonon coupling parameters and time. Figure 4c displays the corresponding heat current and temperature gradient. With the increase of EPI strength, the heat current gradually increases, whereas the temperature gradient decreases. As shown in Figure 4d, the thermal conductivity of Cu−PE increases with the increase of EPI strength, which results from the reduced thermal resistance related to nonequilibrium effects between electrons and phonons. Our results are consistent with Ruan's work,[55] which indicates that traditional MD simulation fails to consider the role of free electrons. In addition, EPI is beneficial to thermal transport of polymer nanocomposites in metals.

The temperature distribution of electrons and phonons for Cu versus EPI strength is shown in Figure 5. Figure 5a,d displays the temperature distribution under two extreme limits,

https://dx.doi.org/10.1021/acs.jpcc.0c07489
J. Phys. Chem. C 2020, 124, 26001−26011

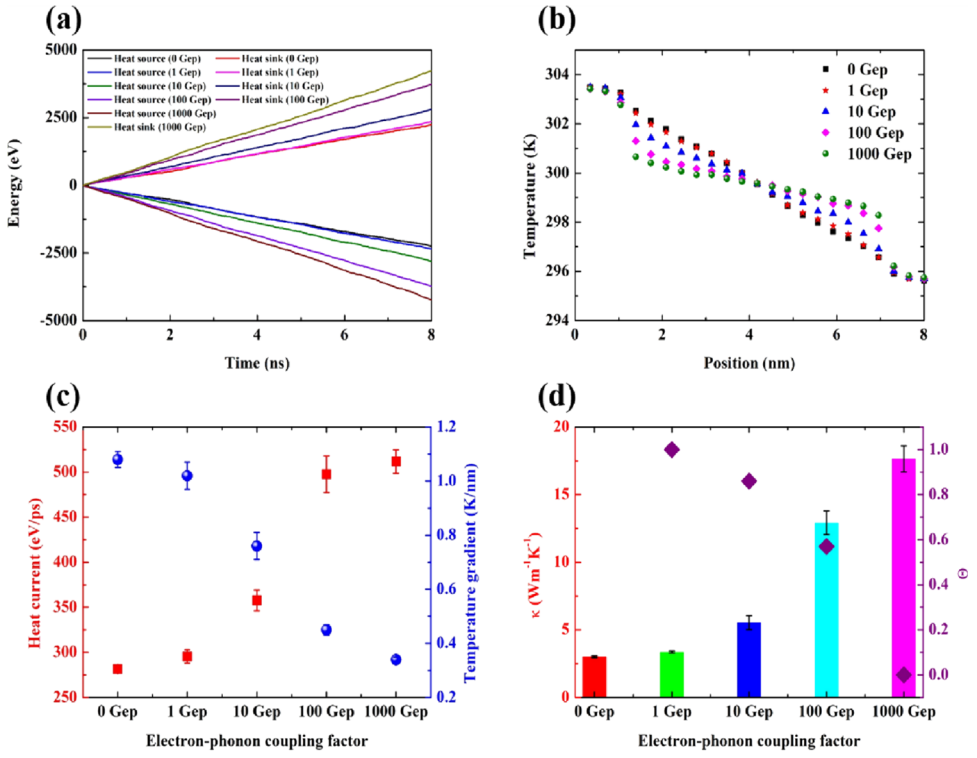

Figure 4. (a) Energy tallies of heat reservoirs as a function of time and electron−phonon coupling. (b) Steady-state temperature distribution as a function of time and electron−phonon coupling. (c) Heat current and temperature gradient as functions of electron−phonon coupling. (d) Thermal conductivity and electron−phonon nonequilibrium characteristic number of Cu−PE as functions of electron−phonon coupling.

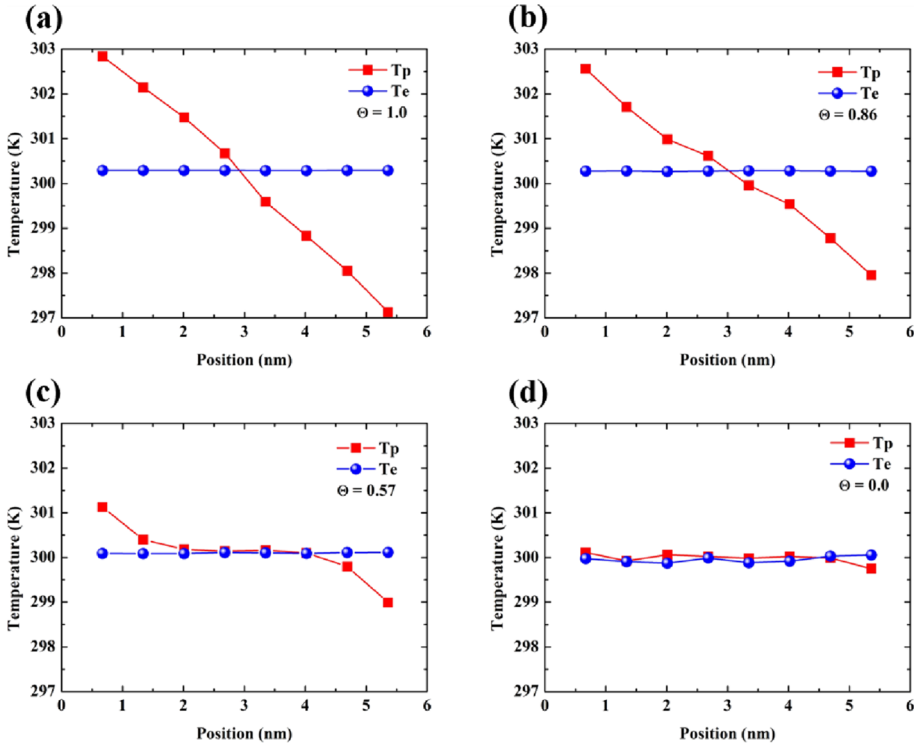

Figure 5. Extracted temperature distribution of electrons and phonons for Cu with different electron−phonon coupling parameters: (a) 1 G_{ep}, (b) 10 G_{ep}, (3) 100 G_{ep}, and (d) 1000 G_{ep}.

that is, Θ approaches to 1 and 0. When Θ approaches to 1, there is a negligible temperature difference among electrons. Thus, electrons make little contribution to thermal transport and neglecting electrons cannot lead to significant errors. Similarly, Hu et al. have observed that measured thermal conductivity by the time-domain thermoreflectance (TDTR) method and calculated thermal conductivity by variance-reduced Monte Carlo simulation without considering electrons

https://dx.doi.org/10.1021/acs.jpcc.0c07489
J. Phys. Chem. C 2020, 124, 26001−26011

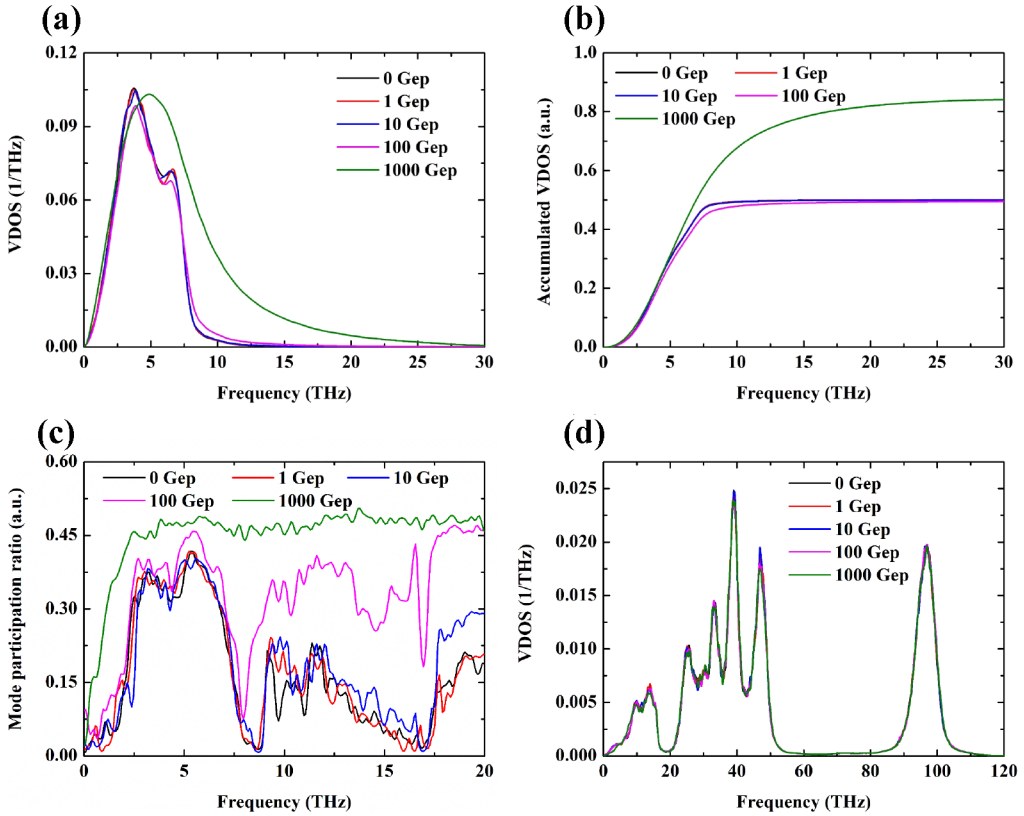

Figure 6. (a) Normalized VDOS of Cu as a function of the electron−phonon coupling parameter. (b) Accumulated normalized VDOS of Cu as a function of the electron−phonon coupling parameter. (c) Mode participation ratio of Cu as a function of the electron−phonon coupling parameter. (d) Normalized VDOS of PE as a function of the electron−phonon coupling parameter.

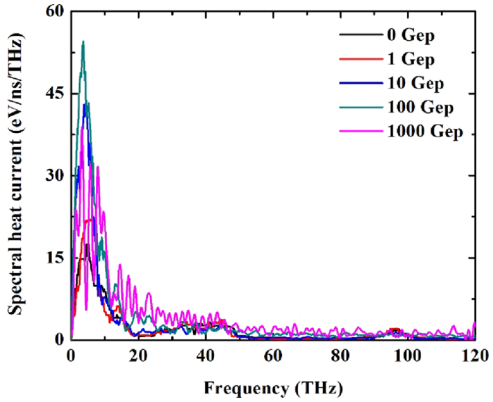

Figure 7. Corrected spectral heat current as a function of electron−phonon coupling factor.

agree well with each other.[58] Hua et al. also found that measured phonon transmission coefficients by the TDTR approach are consistent with the calculated value by solving the Boltzmann transport equation (BTE) without considering electrons.[59] The same point between Hu's work[58] and Hua's work[59] is that the thickness of the metal film is on the order of 10 nm, which is comparable to the MFP of electrons and EPN length. Thus, their work can be categorized into the situation of Θ close to 1, where neglecting electrons is acceptable. However, as can be clearly seen from Figure 4d, when Θ gradually deviates to 1, the contribution of EPI to thermal transport cannot be neglected. In the view of equivalent thermal circuit, the decrease of R_{EPN} is responsible for the increase of thermal conductivity. Our results demonstrate that the introduced dimensionless number Θ can effectively characterize the EPN degree. Moreover, modulating EPI strength by tuning the electronic structure of the metal is an efficient way to modulate thermal conductivity of polymer nanocomposites.

To unravel the underlying mechanisms, the normalized vibrational density of states (VDOS) and spectral heat current are calculated. Based on the kinetic theory, thermal conductivity can be calculated by

$$\kappa = \frac{1}{3V}\int_0^{\omega_m} \hbar\omega \frac{\partial f_{BE}}{\partial T} v_g(\omega) v_g(\omega) \tau(\omega) \mathrm{VDOS}(\omega) \mathrm{d}\omega \tag{12}$$

where $\hbar$, ω, ω_m, f_{BE}, $v_g(\omega)$, and $\tau(\omega)$ are the reduced Planck's constant, angular frequency, upper limit of integration frequency, Bose−Einstein distribution function, frequency-dependent group velocity, and phonon relaxation time, respectively. The VDOS describes the frequency distribution of phonons and can be calculated by Fourier transforming the normalized velocity autocorrelation function (VACF), which can be written as[60]

$$\mathrm{VDOS}(\omega) = \int_{-\infty}^{+\infty} \frac{<\boldsymbol{v}(0)\cdot\boldsymbol{v}(t)>}{<\boldsymbol{v}(0)\cdot\boldsymbol{v}(0)>} \cos(\omega t)\mathrm{d}t \tag{13}$$

where $\frac{<\boldsymbol{v}(0)\cdot\boldsymbol{v}(t)>}{<\boldsymbol{v}(0)\cdot\boldsymbol{v}(0)>}$ is the normalized VACF. The VACF of Cu and PE is shown in Figure S4, which decays to 0 within the correlation time of 2.5 ps. The mode participation ratio (MPR) can be calculated by[50]

https://dx.doi.org/10.1021/acs.jpcc.0c07489
J. Phys. Chem. C 2020, 124, 26001−26011

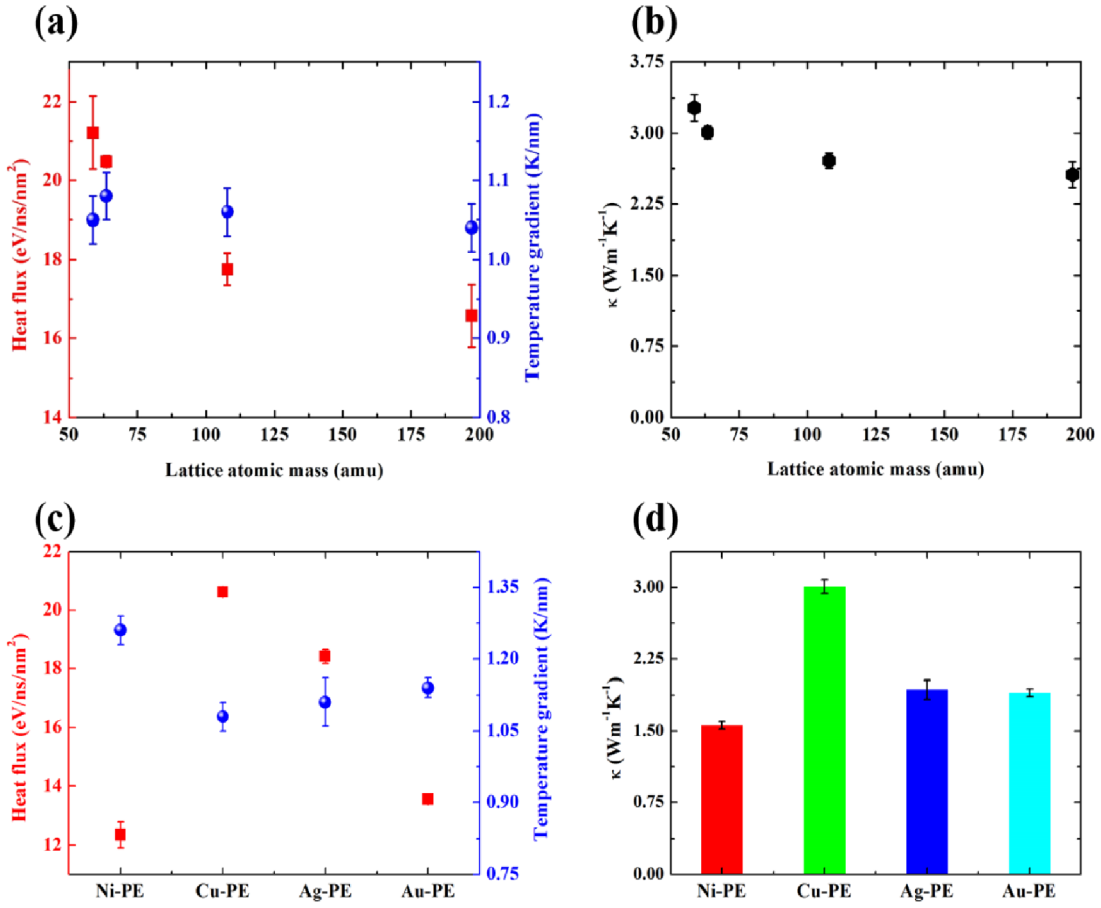

Figure 8. (a) Heat flux and temperature gradient as functions of lattice atomic mass. (b) Thermal conductivity of Cu−PE as a function of lattice atomic mass. (c) Heat flux and temperature gradient of PE nanocomposites with different fillers. (d) Thermal conductivity of PE nanocomposites with different fillers.

$$\mathrm{MPR}(\omega) = \frac{1}{N}\frac{\left(\sum_i \mathrm{VDOS}_i(\omega)^2\right)^2}{\sum_i \mathrm{VDOS}_i(\omega)^4} \tag{14}$$

where N is the number of atoms in the system, $\mathrm{VDOS}_i(\omega)$ is the local VDOS of the i-th atom. As shown in Figure 6a,b, with the increase of EPI interaction, the normalized VDOS of Cu is broadened, which indicates that more phonons of Cu are excited. In addition, Figure 6c shows that the MPR of Cu increases with the increase of EPI, which indicates phonons of Cu become more delocalized.

Figure 6d shows that phonons of PE occur little change. The VDOS only reflects the harmonic property, but anharmonic property plays an important role in thermal transport at room temperature. The anharmonic property originates from the nonlinear interatomic force, and thus, spectral heat current can reflect thermal transport induced by the anharmonic interaction.

Sääskilahti et al. propose to decompose heat current at the frequency level, which can be given by[61]

$$\tilde{K}(\omega) = \frac{2}{M\Delta t_s}\left| Re\sum_{i\in L}\sum_{j\in R} \boldsymbol{F}_{ij}(\omega)\cdot\boldsymbol{v}_i(\omega)^* \right| \tag{15}$$

where Δt_s and M are the sampling interval and the number of samples. Here, we choose Δt_s and M to ensure the force−velocity correlation function to attenuate to zero in the correlation time. It is challenging for us to accurately determine the interatomic force ($\boldsymbol{F}_{ij}$). Therefore, the finite difference algorithm is used to combine with LAMMPS,[51] which is the major source of error for spectral heat current. The inverse Fourier transformation of spectral heat current is

$$K(t) = \int_{-\infty}^{+\infty} \frac{d\omega}{2\pi} e^{-i\omega t}\tilde{K}(\omega) \tag{16}$$

At zero correlation time, the spectral heat current should reduce to the nonequilibrium heat current. Hence, the corrected spectral heat current can be written as

$$\tilde{K}(\omega)_c = \tilde{K}(\omega)\frac{Q}{\int_{-\infty}^{+\infty}\frac{d\omega}{2\pi}\tilde{K}(\omega)} \tag{17}$$

Figure 7 depicts that the heat current contributed by low-frequency phonons is gradually enhanced with the increase of EPI. Moreover, when the EPI continues to increase from 100 Gep to 1000 Gep, the heat current contributed by mid-frequency and high-frequency phonons is also enhanced. Because high-frequency phonons are more likely to be localized, we ascribe this to the enhanced phonon hopping.

3.3. Effects of the Atomic Mass Modification. Atomic mass modification is a feasible way to investigate the impacts of impurity on thermal conductivity.[26] Here, the relationship between thermal conductivity and atomic mass of lattice is studied by modifying the atomic mass in the EAM potential. The atomic mass of lattice is changed to 58.69, 107.87, and

https://dx.doi.org/10.1021/acs.jpcc.0c07489
J. Phys. Chem. C 2020, 124, 26001−26011

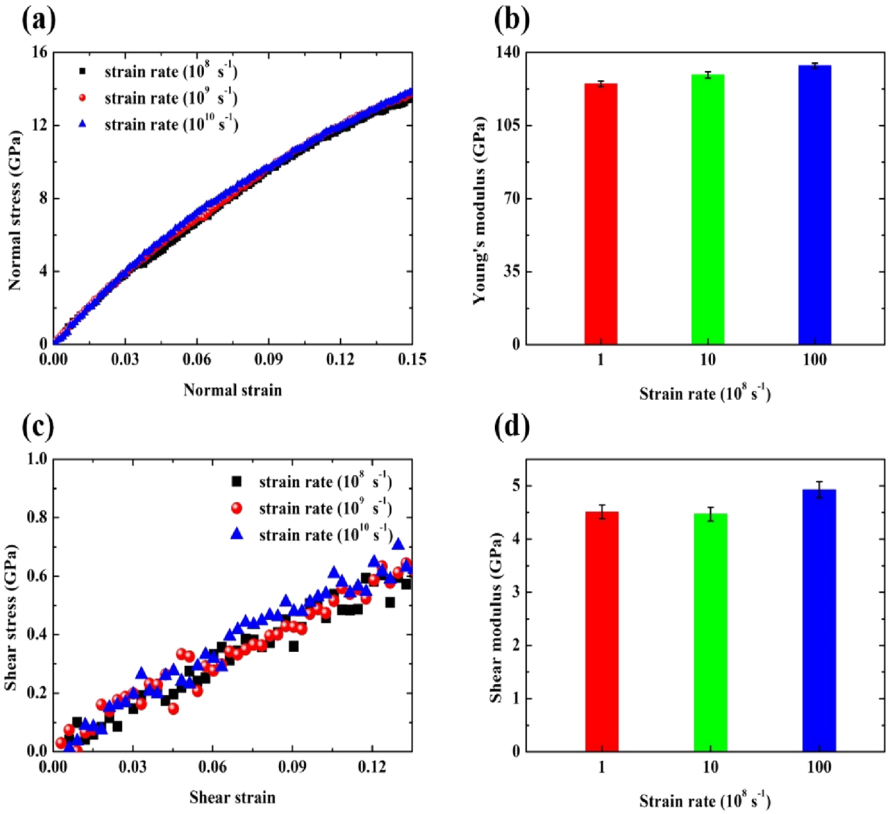

Figure 9. (a) Normal stress as a function of normal strain and strain rate. (b) Young's modulus as a function of strain rate. (c) Shear stress as a function of shear strain and strain rate. (d) Shear modulus as a function of strain rate.

196.97, which correspond to the atomic mass of Ni, Ag, and Au. The NEMD simulations of Ni−PE, Ag−PE, and Au−PE are conducted to compare. The heat flux, temperature gradient, and thermal conductivity with respect to the atomic mass of lattice are shown in Figure 8a,b. The fluctuation of the temperature gradient is negligible, but the heat flux decreases with the increase of lattice atomic mass. Hence, a modest decrease in thermal conductivity occurs, which is related to the increased phonon scattering. The corresponding heat flux, temperature gradient, and thermal conductivity of PE nanocomposites are shown in Figure 8c,d, which indicates that the thermal conductivity strongly depends on the filler property.

3.4. Effects of Strain Rates on Mechanical Property. The mechanical property of the material is a crucial characteristic in real applications, and the strain rate is also a crucial factor in processing polymers. Here, the effects of strain rates on the mechanical property of Cu-PE are investigated. Three strain rates including 10^8, 10^9, and 10^{10} s^{-1} are chosen, and the stress is calculated by[62]

$$\sigma_{\alpha\beta} = \frac{1}{V}\left(\sum_{i=1}^{N} m_i v_\alpha^i v_\beta^i + \frac{1}{2}\sum_{i=1}^{N-1}\sum_{j=i+1}^{N} r_{ij,\alpha} F_{ij,\beta}\right) \quad (18)$$

where N, α, and β stand for the number of atoms in the system and the components of the Cartesian coordinate. The mechanical modulus can be calculated by linear fitting the stress−strain curves, which can be given by[63]

$$K_{\alpha\beta} = \left.\frac{d\sigma_{\alpha\beta}}{d\varepsilon_{\alpha\beta}}\right|_{\varepsilon_{\alpha\beta}\to 0} \quad (19)$$

Frequency-dependent phonon relaxation time follows a scaling law of $\tau(\omega) \sim \omega^{-\xi}$ due to different phonon scattering mechanisms. For polymer nanocomposites, phonon relaxation time declines dramatically with the increase of phonon frequency due to the intensified phonon scattering. Hence, low-frequency acoustic phonons are the main heat carriers. According to the Debye approximation, in the low-frequency limit, the lattice vibration wave can be regarded as the elastic wave and the phonon angular frequency follows a linear relation with a wave vector of $\omega = v_g|\boldsymbol{k}|$. Thus, the phonon group velocity is equal to the sound velocity:

$$v_L \approx \sqrt{\frac{Y}{\rho}} \text{ and } v_T \approx \sqrt{\frac{G}{\rho}} \quad (20)$$

where v_L, v_T, Y, G, and ρ are the phonon group velocity of longitudinal mode and transverse mode, Young's modulus, shear modulus, and density, respectively. In this regard, a higher mechanical modulus leads to a higher phonon velocity and facilitate thermal transport. Figure 9 shows the stress−strain curves and corresponding mechanical modulus. Similar to diamond, PE chains are also made up of strong carbon−carbon bonds and the low Young's modulus of bulk polymers stems from the defects like vacancy, impurity, and so on. The Young's modulus of PE chains can be as high as 330.7 GPa,[24] which leads to the high Young's modulus of Cu−PE (~125 GPa). Due to the impacts of nanopores, the shear modulus of Cu−PE is around 4.5 GPa. Higher strain rates can only slightly influence the mechanical modulus. Thus, using strain to enhance thermal conductivity of polymers should combine the enhancement of mechanical modulus and polymer chain orientation.

https://dx.doi.org/10.1021/acs.jpcc.0c07489
J. Phys. Chem. C 2020, 124, 26001−26011

4. CONCLUSIONS

To summarize, using a Cu−PE system as a model, we investigated the impacts of filler length, filler property, electron−phonon coupling, and impurity on thermal conductivity by combining NEMD simulations with the TTM. By analogy to the Knudsen number, the EPN characteristic number Θ is defined to evaluate the EPN degree. The equivalent thermal circuit reveals that both the nonlocal and nonequilibrium effects of heat carriers hinder thermal transport. Through reducing nonlocal effects and nonequilibrium effects, the thermal conductivity of Cu−PE can be 122.13 W m^{-1} K^{-1}. When the length of Cu−PE is fixed, reducing the EPN degree can increase the thermal conductivity by four times. Phonon spectra and spectral heat current demonstrate that more low-frequency phonons are excited and contribute more to thermal transport with the increase of EPI strength. In addition, impurities with larger atomic mass reduce thermal conductivity more and the impact of strain rates on the mechanical modulus is small.

■ ASSOCIATED CONTENT

Supporting Information

The Supporting Information is available free of charge at https://pubs.acs.org/doi/10.1021/acs.jpcc.0c07489.

The main and lateral views, schematic diagram of building the initial structure, the evolution process, and the structural parameters of the Cu−PE system and the detailed description and parameters of the potential energy function (PDF)

■ AUTHOR INFORMATION

Corresponding Author

Zhichun Liu − *School of Energy and Power Engineering, Huazhong University of Science and Technology (HUST), Wuhan 430074, China;* orcid.org/0000-0001-9645-3052; Email: zcliu@hust.edu.cn

Authors

Bo Zhang − *School of Energy and Power Engineering, Huazhong University of Science and Technology (HUST), Wuhan 430074, China*

Yunmin Liang − *School of Energy and Power Engineering, Huazhong University of Science and Technology (HUST), Wuhan 430074, China*

Wei Liu − *School of Energy and Power Engineering, Huazhong University of Science and Technology (HUST), Wuhan 430074, China*

Complete contact information is available at: https://pubs.acs.org/10.1021/acs.jpcc.0c07489

Notes

The authors declare no competing financial interest.

■ ACKNOWLEDGMENTS

The authors are grateful to Peng Liu, Quanwen Liao, Xiaoxiang Yu, Meng An, Nuo Yang, and Wenjiang Zhou for useful discussions. This work was supported by the National Natural Science Foundation of China (Grant no. 51776079) and the National Key Research and Development Program of China (no. 2017YFB0603501-3). The work was carried out at the National Supercomputer Center in Tianjin, and the calculations were performed on TianHe-1(A).

■ REFERENCES

(1) Huang, C.; Qian, X.; Yang, R. Thermal conductivity of polymers and polymer nanocomposites. *Mater. Sci. Eng., R Rep.* **2018**, *132*, 1−22.

(2) Zhang, B.; Mao, P.; Liang, Y.; He, Y.; Liu, W.; Liu, Z. Modulating Thermal Transport in Polymers and Interfaces: Theories, Simulations, and Experiments. *ES Energy Environ.* **2019**, *5*, 37−55.

(3) Xu, X.; Chen, J.; Zhou, J.; Li, B. Thermal Conductivity of Polymers and Their Nanocomposites. *Adv. Mater.* **2018**, *30*, 1705544.

(4) Cahill, D. G.; Braun, P. V.; Chen, G.; Clarke, D. R.; Fan, S.; Goodson, K. E.; Keblinski, P.; King, W. P.; Mahan, G. D.; et al. Nanoscale thermal transport. II. 2003−2012. *Appl. Phys. Rev.* **2014**, *1*, No. 011305.

(5) Yu, W.; Liu, C.; Qiu, L.; Zhang, P.; Ma, W.; Yue, Y.; Xie, H.; Larkin, L. S. Advanced Thermal Interface Materials for Thermal Management. *Eng. Sci.* **2018**, *2*, 1−3.

(6) Mehra, N.; Mu, L.; Ji, T.; Yang, X.; Kong, J.; Gu, J.; Zhu, J. Thermal transport in polymeric materials and across composite interfaces. *Appl. Mater. Today* **2018**, *12*, 92−130.

(7) Tong, Z.; Li, S.; Ruan, X.; Bao, H. Comprehensive first-principles analysis of phonon thermal conductivity and electron-phonon coupling in different metals. *Phys. Rev. B* **2019**, *100*, 144306.

(8) Giri, A.; Tokina, M. V.; Prezhdo, O. V.; Hopkins, P. E. Electron−phonon coupling and related transport properties of metals and intermetallic alloys from first principles. *Mater. Today Phys.* **2020**, *12*, 100175.

(9) Lin, Z.; Zhigilei, L. V.; Celli, V. Electron-phonon coupling and electron heat capacity of metals under conditions of strong electron-phonon nonequilibrium. *Phys. Rev. B* **2008**, *77*, No. 075133.

(10) Qiu, T. Q.; Tien, C. L. Short-pulse laser heating on metals. *Int. J. Heat Mass Transfer* **1992**, *35*, 719−726.

(11) Xu, S.; Fan, A.; Wang, H.; Zhang, X.; Wang, X. Raman-based Nanoscale Thermal Transport Characterization: A Critical Review. *Int. J. Heat Mass Transfer* **2020**, *154*, 119751.

(12) Ma, W.; Zhang, X. Study of the thermal, electrical and thermoelectric properties of metallic nanofilms. *Int. J. Heat Mass Transfer* **2013**, *58*, 639−651.

(13) Ma, W. G.; Wang, H. D.; Zhang, X.; Wang, W. Experiment study of the size effects on electron-phonon relaxation and electrical resistivity of polycrystalline thin gold films. *J. Appl.Phys.* **2010**, *108*, No. 064308.

(14) Groeneveld, R. H. M.; Sprik, R.; Lagendijk, A. Femtosecond spectroscopy of electron-electron and electron-phonon energy relaxation in Ag and Au. *Phys. Rev. B* **1995**, *51*, 11433−11445.

(15) Liu, T.-H.; Zhou, J.; Liao, B.; Singh, D. J.; Chen, G. First-principles mode-by-mode analysis for electron-phonon scattering channels and mean free path spectra in GaAs. *Phys. Rev. B* **2017**, *95*, No. 075206.

(16) Xu, Q.; Zhou, J.; Liu, T.-H.; Chen, G. Effect of electron-phonon interaction on lattice thermal conductivity of SiGe alloys. *Appl. Phys. Lett.* **2019**, *115*, No. 023903.

(17) Vallabhaneni, A. K.; Singh, D.; Bao, H.; Murthy, J.; Ruan, X. Reliability of Raman measurements of thermal conductivity of single-layer graphene due to selective electron-phonon coupling: A first-principles study. *Phys. Rev. B* **2016**, *93*, 125432.

(18) Yang, N.; Luo, T.; Esfarjani, K.; Henry, A.; Tian, Z.; Shiomi, J.; Chalopin, Y.; Li, B.; Chen, G. Thermal Interface Conductance Between Aluminum and Silicon by Molecular Dynamics Simulations. *J. Comput. Theor. Nanosci.* **2015**, *12*, 168−174.

(19) Henry, A.; Chen, G. High Thermal Conductivity of Single Polyethylene Chains Using Molecular Dynamics Simulations. *Phys. Rev. Lett.* **2008**, *101*, 235502.

(20) Henry, A.; Chen, G. Anomalous heat conduction in polyethylene chains: Theory and molecular dynamics simulations. *Phys. Rev. B* **2009**, *79*, 144305.

(21) Henry, A.; Chen, G.; Plimpton, S. J.; Thompson, A. 1D-to-3D transition of phonon heat conduction in polyethylene using molecular dynamics simulations. *Phys. Rev. B* **2010**, *82*, 144308.

(22) Liu, J.; Yang, R. Length-dependent thermal conductivity of single extended polymer chains. *Phys. Rev. B* **2012**, *86*, 104307.
(23) Liu, J.; Yang, R. Tuning the thermal conductivity of polymers with mechanical strains. *Phys. Rev. B* **2010**, *81*, 174122.
(24) Wang, X.; Kaviany, M.; Huang, B. Phonon coupling and transport in individual polyethylene chains: a comparison study with the bulk crystal. *Nanoscale* **2017**, *9*, 18022−18031.
(25) Shulumba, N.; Hellman, O.; Minnich, A. J. Lattice Thermal Conductivity of Polyethylene Molecular Crystals from First-Principles Including Nuclear Quantum Effects. *Phys. Rev. Lett.* **2017**, *119*, 185901.
(26) Liao, Q.; Zeng, L.; Liu, Z.; Liu, W. Tailoring Thermal Conductivity of Single-stranded Carbon-chain Polymers through Atomic Mass Modification. *Sci. Rep.* **2016**, *6*, 34999.
(27) Liao, Q.; Liu, Z.; Liu, W.; Deng, C.; Yang, N. Extremely High Thermal Conductivity of Aligned Carbon Nanotube-Polyethylene Composites. *Sci. Rep.* **2015**, *5*, 16543.
(28) Tu, R.; Liao, Q.; Zeng, L.; Liu, Z.; Liu, W. Impact of torsion and stretching on the thermal conductivity of polyethylene strands. *Appl. Phys. Lett.* **2017**, *110*, 101905.
(29) Ma, H.; Tian, Z. Effects of polymer topology and morphology on thermal transport: A molecular dynamics study of bottlebrush polymers. *Appl. Phys. Lett.* **2017**, *110*, No. 091903.
(30) Ma, H.; Tian, Z. Significantly High Thermal Rectification in an Asymmetric Polymer Molecule Driven by Diffusive versus Ballistic Transport. *Nano Lett.* **2018**, *18*, 43−48.
(31) Luo, D.; Huang, C.; Huang, Z. Decreased Thermal Conductivity of Polyethylene Chain Influenced by Short Chain Branching. *J. Heat Transfer* **2017**, *140*, No. 031302.
(32) Zhang, T.; Wu, X.; Luo, T. Polymer Nanofibers with Outstanding Thermal Conductivity and Thermal Stability: Fundamental Linkage between Molecular Characteristics and Macroscopic Thermal Properties. *J. Phys. Chem. C* **2014**, *118*, 21148−21159.
(33) Wei, X.; Luo, T. Chain length effect on thermal transport in amorphous polymers and a structure−thermal conductivity relation. *Phys. Chem. Chem. Phys.* **2019**, *21*, 15523−15530.
(34) Zhang, T.; Luo, T. Role of Chain Morphology and Stiffness in Thermal Conductivity of Amorphous Polymers. *J. Phys. Chem. B* **2016**, *120*, 803−812.
(35) Yu, X.; Li, R.; Shiga, T.; Feng, L.; An, M.; Zhang, L.; Shiomi, J.; Yang, N. Hybrid Thermal Transport Characteristics of Doped Organic Semiconductor Poly(3,4-ethylenedioxythiophene):Tosylate. *J. Phys. Chem. C* **2019**, *123*, 26735−26741.
(36) Li, S.; Yu, X.; Bao, H.; Yang, N. High Thermal Conductivity of Bulk Epoxy Resin by Bottom-Up Parallel-Linking and Strain: A Molecular Dynamics Study. *J. Phys. Chem. C* **2018**, *122*, 13140−13147.
(37) An, M.; Demir, B.; Wan, X.; Meng, H.; Yang, N.; Walsh, T. R. Predictions of Thermo-Mechanical Properties of Cross-Linked Polyacrylamide Hydrogels Using Molecular Simulations. *Adv. Theory Simul.* **2019**, *2*, 1800153.
(38) Meng, H.; Yu, X.; Feng, H.; Xue, Z.; Yang, N. Superior thermal conductivity of poly (ethylene oxide) for solid-state electrolytes: A molecular dynamics study. *Int. J. Heat Mass Transfer* **2019**, *137*, 1241−1246.
(39) Shen, S.; Henry, A.; Tong, J.; Zheng, R.; Chen, G. Polyethylene nanofibres with very high thermal conductivities. *Nat. Nanotechnol.* **2010**, *5*, 251−255.
(40) Shrestha, R.; Li, P.; Chatterjee, B.; Zheng, T.; Wu, X.; Liu, Z.; Luo, T.; Choi, S.; Hippalgaonkar, K.; de Boer, M. P.; Shen, S. Crystalline polymer nanofibers with ultra-high strength and thermal conductivity. *Nat. Commun.* **2018**, *9*, 1664.
(41) Xu, Y.; Kraemer, D.; Song, B.; Jiang, Z.; Zhou, J.; Loomis, J.; Wang, J.; Li, M.; Ghasemi, H.; Huang, X.; et al. Nanostructured polymer films with metal-like thermal conductivity. *Nat. Commun.* **2019**, *10*, 1771.
(42) Zhang, Y.; Zhang, X.; Yang, L.; Zhang, Q.; Fitzgerald, M. L.; Ueda, A.; Chen, Y.; Mu, R.; Li, D.; Bellan, L. M. Thermal transport in electrospun vinyl polymer nanofibers: effects of molecular weight and side groups. *Soft Matter* **2018**, *14*, 9534−9541.
(43) Ma, J.; Zhang, Q.; Mayo, A.; Ni, Z.; Yi, H.; Chen, Y.; Mu, R.; Bellan, L. M.; Li, D. Thermal conductivity of electrospun polyethylene nanofibers. *Nanoscale* **2015**, *7*, 16899−16908.
(44) Mu, L.; He, J.; Li, Y.; Ji, T.; Mehra, N.; Shi, Y.; Zhu, J. Molecular Origin of Efficient Phonon Transfer in Modulated Polymer Blends: Effect of Hydrogen Bonding on Polymer Coil Size and Assembled Microstructure. *J. Phys. Chem. C* **2017**, *121*, 14204−14212.
(45) Zhang, L.; Ruesch, M.; Zhang, X.; Bai, Z.; Liu, L. Tuning thermal conductivity of crystalline polymer nanofibers by interchain hydrogen bonding. *RSC Adv.* **2015**, *5*, 87981−87986.
(46) Robbins, A. B.; Drakopoulos, S. X.; Martin-Fabiani, I.; Ronca, S.; Minnich, A. J. Ballistic thermal phonons traversing nanocrystalline domains in oriented polyethylene. *Proc. Natl. Acad. Sci. U. S. A.* **2019**, *116*, 17163.
(47) Xie, X.; Li, D.; Tsai, T.-H.; Liu, J.; Braun, P. V.; Cahill, D. G. Thermal Conductivity, Heat Capacity, and Elastic Constants of Water-Soluble Polymers and Polymer Blends. *Macromolecules* **2016**, *49*, 972−978.
(48) Cao, B.-Y.; Li, Y.-W.; Kong, J.; Chen, H.; Xu, Y.; Yung, K.-L.; Cai, A. High thermal conductivity of polyethylene nanowire arrays fabricated by an improved nanoporous template wetting technique. *Polymer* **2011**, *52*, 1711−1715.
(49) Kodama, T.; Ohnishi, M.; Park, W.; Shiga, T.; Park, J.; Shimada, T.; Shinohara, H.; Shiomi, J.; Goodson, K. E. Modulation of Thermal and Thermoelectric Transport in Individual Carbon Nanotubes by Fullerene Encapsulation. *Nat. Mater.* **2017**, *16*, 892−897.
(50) Bao, H.; Chen, J.; Gu, X.; Cao, B. A Review of Simulation Methods in Micro/Nanoscale Heat Conduction. *ES Energy Environ.* **2018**, *1*, 16−55.
(51) Plimpton, S. Fast Parallel Algorithms for Short-Range Molecular Dynamics. *J. Comput. Phys.* **1995**, *117*, 1−19.
(52) Foiles, S. M.; Baskes, M. I.; Daw, M. S. Embedded-atom-method functions for the fcc metals Cu, Ag, Au, Ni, Pd, Pt, and their alloys. *Phys. Rev. B* **1986**, *33*, 7983−7991.
(53) Sun, H.; Mumby, S. J.; Maple, J. R.; Hagler, A. T. An ab Initio CFF93 All-Atom Force Field for Polycarbonates. *J. Am. Chem. Soc.* **1994**, *116*, 2978−2987.
(54) Rappe, A. K.; Casewit, C. J.; Colwell, K. S.; Goddard, W. A.; Skiff, W. M. UFF, a full periodic table force field for molecular mechanics and molecular dynamics simulations. *J. Am. Chem. Soc.* **1992**, *114*, 10024−10035.
(55) Wang, Y.; Ruan, X.; Roy, A. K. Two-temperature non-equilibrium molecular dynamics simulation of thermal transport across metal-nonmetal interfaces. *Phys. Rev. B* **2012**, *85*, 205311.
(56) Lu, Z.; Wang, Y.; Ruan, X. Metal/dielectric thermal interfacial transport considering cross-interface electron-phonon coupling: Theory, two-temperature molecular dynamics, and thermal circuit. *Phys. Rev. B* **2016**, *93*, No. 064302.
(57) Sverdrup, P. G.; Sinha, S.; Asheghi, M.; Uma, S.; Goodson, K. E. Measurement of Ballistic Phonon Conduction near Hotspots in Silicon. *Appl. Phys. Lett.* **2001**, *78*, 3331−3333.
(58) Hu, Y.; Zeng, L.; Minnich, A. J.; Dresselhaus, M. S.; Chen, G. Spectral mapping of thermal conductivity through nanoscale ballistic transport. *Nat. Nanotechnol.* **2015**, *10*, 701−706.
(59) Hua, C.; Chen, X.; Ravichandran, N. K.; Minnich, A. J. Experimental metrology to obtain thermal phonon transmission coefficients at solid interfaces. *Phys. Rev. B* **2017**, *95*, 205423.
(60) Dickey, J. M.; Paskin, A. Computer Simulation of the Lattice Dynamics of Solids. *Phys. Rev.* **1969**, *188*, 1407−1418.
(61) Sääskilahti, K.; Oksanen, J.; Tulkki, J.; Volz, S. Spectral mapping of heat transfer mechanisms at liquid-solid interfaces. *Phys. Rev. E* **2016**, *93*, No. 052141.
(62) Liu, T.-H.; Pao, C.-W.; Chang, C.-C. Effects of dislocation densities and distributions on graphene grain boundary failure strengths from atomistic simulations. *Carbon* **2012**, *50*, 3465−3472.

https://dx.doi.org/10.1021/acs.jpcc.0c07489
J. Phys. Chem. C 2020, 124, 26001−26011

(63) Zhang, B.; Li, J.; Gao, S.; Liu, W.; Liu, Z. Comparison of Thermomechanical Properties for Weaved Polyethylene and Its Nanocomposite Based on the CNT Junction by Molecular Dynamics Simulation. *J. Phys. Chem. C* **2019**, *123*, 19412−19420.

https://dx.doi.org/10.1021/acs.jpcc.0c07489
J. Phys. Chem. C 2020, 124, 26001−26011